Clays and Clay Minerals, Vol. 58, No. 5, 627–643, 2010.

ELEMENT DISTRIBUTION BETWEEN COEXISTING AUTHIGENIC MINERAL PHASES IN ARGILLIC AND ZEOLITIC ALTERED TEPHRA, OLDUVAI GORGE, TANZANIA

LINDSAY J. MCHENRY*

Department of Geosciences, University of Wisconsin-Milwaukee, 3209 N. Maryland Ave, Milwaukee, WI 53211, USA

Abstract—The current study demonstrates how co-existing zeolite and clay minerals formed by the alteration of tephra in a closed-basin lacustrine and lake-margin environment can retain the overall composition of the original bulk tephra for many elements, even when diagenetic conditions and resulting authigenic mineral assemblages change. Zeolite and clay minerals co-exist in the closed-basin, saline-alkaline lacustrine altered tephra of Pleistocene Olduvai Gorge, Tanzania, and their diagenetic histories can be reconstructed using variations in their textures and compositions. The authigenic minerals in the altered tephra of the Olduvai paleolake form a classic 'bull's-eye' pattern, with clay-dominated tephra in the distal lake margin, chabazite and phillipsite in the proximal margin, and phillipsite ± K-feldspar in the intermittently dry lake and lake center. Fifteen representative samples of altered volcanic ash lapilli (designated Tuff IF) were analyzed by X-ray diffraction (XRD), X-ray fluorescence (XRF), electron probe microanalysis (EPMA), and scanning electron microscopy (SEM) to determine their authigenic mineral assemblages and bulk compositions, and to texturally and compositionally compare their clay mineral and zeolite components.

Textural observations indicate that clay minerals formed first, followed by zeolites and finally feldspars. Clay minerals, however, persist even in the most altered samples. The overall composition of Tuff IF shows only limited change in Fe, Si, Al, and Na between fresh, clay-altered, and zeolite-dominated diagenetic environments, despite significant differences in authigenic assemblage. Where zeolites dominate the assemblage, the remaining clay minerals are rich in Mg, Fe, and Ti, elements that are not readily incorporated in zeolite structures. Where clay minerals dominate, they are more Al-rich. A 'mixing model' combining clay-mineral and zeolite compositions yields a close approximation of the original volcanic glass for most elements (exceptions including Mg, Ca, and K). This initial composition was preserved in part by the redistribution of elements between co-existing clay minerals and zeolites.

Key Words—Clay, Diagenesis, Element Partitioning, Olduvai Gorge, Phillipsite, Saline-alkaline Lake, Smectite, Tephra, Zeolite.

INTRODUCTION

Olduvai Gorge in northern Tanzania exposes sediments associated with a Pliocene-Pleistocene saline-alkaline lake, including abundant zeolitically and argillically altered tephra derived from the nearby Ngorongoro Volcanic Highlands (NVH, Figure 1). Hay studied the zeolitic Olduvai tephra in detail (*e.g.* Hay, 1963, 1964, 1970, 1973, 1976, 1980, 1986, 1996; Hay and Kyser, 2001), identifying the phases and assemblages present and delineating lacustrine, intermittently dry lacustrine, and lake-margin environments based, in part, on sedimentology and authigenic mineralogy (Figure 2). Mees *et al.* (2005, 2007), Deocampo *et al.* (2002), Deocampo (2004), Hover and Ashley (2003), and McHenry (2009) have continued this work, using the authigenic mineral assemblages (both clay and zeolite) to help reconstruct the conditions during the deposition and diagenesis of the Olduvai beds. This long history of studies of authigenic mineralization in the Olduvai basin provides a context for more targeted analyses of specific diagenetic processes and patterns.

Zeolites commonly form as alteration products of volcanic materials, especially in closed-basin saline-alkaline lakes such as at Pliocene-Pleistocene Olduvai. The authigenic mineral assemblage formed provides information about the diagenetic conditions, as different authigenic minerals require different ranges of pH, salinity, temperature, and starting composition (Sheppard and Hay, 2001). Zeolite minerals do not form alone. Smectites and other clay minerals are common accessory phases, hosting elements from the original volcanic glass that do not fit as easily into the zeolite structure.

The diagenetic conditions, and resulting authigenic mineral assemblages, vary spatially within a closed-basin lacustrine environment. Fresh or clay-altered glass can persist in the outer edges of the basin and above the water table, whereas zeolites commonly dominate the central basin (*e.g.* Dibble and Tiller, 1981; Hay, 1986). The authigenic minerals often form a 'bull's-eye' pattern, with smectite and zeolites characteristic of less

* E-mail address of corresponding author:
lmchenry@uwm.edu
DOI: 10.1346/CCMN.2010.0580504

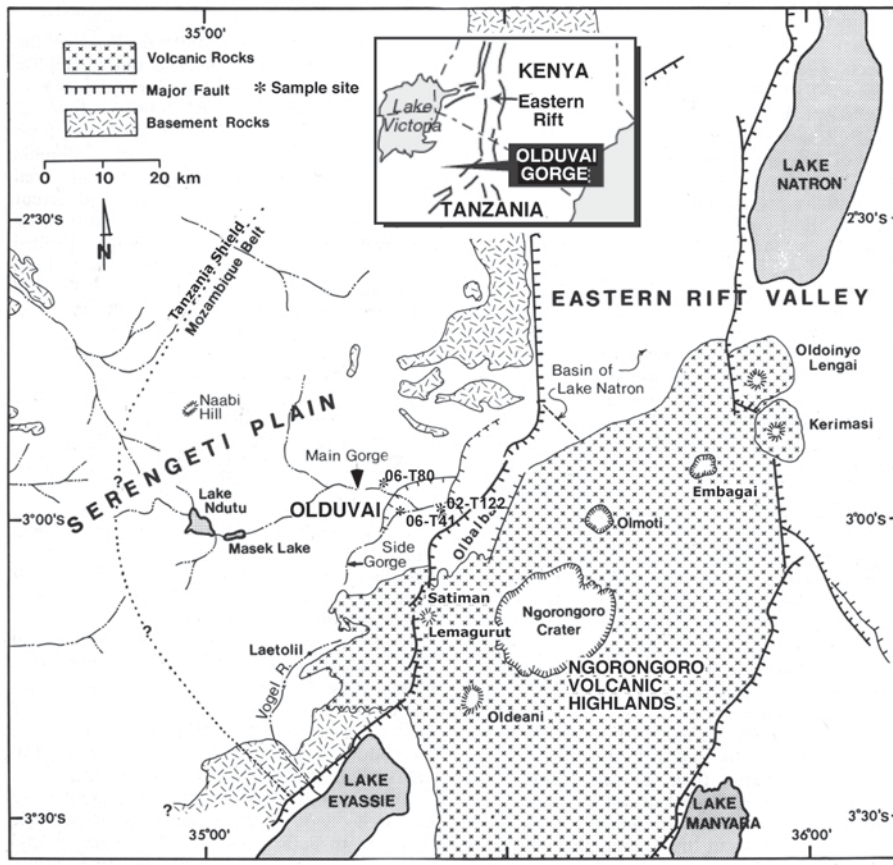

Figure 1. Regional map showing location of Olduvai Gorge. Tephra were derived from the Ngorongoro Volcanic Highlands (NVH) to the east. The positions of three samples in the Olduvai basin are indicated. Map after Hay (1976).

saline-alkaline conditions (*e.g.* chabazite) near the margins and phillipsite, authigenic K-feldspar, and analcime near the center (*e.g.* Hay, 1986; Ming and Mumpton, 1989; Hay and Sheppard, 2001).

Many previous studies of zeolitized tephra have focused nearly exclusively on the zeolites, paying less attention to the ubiquitous (yet sometimes minor) clay and other minerals that form with them. Considering these other phases is important when addressing changes in bulk chemistry and the contributions of the diagenetic fluids, because they can concentrate elements that are incompatible within a zeolite structure. Olduvai Gorge is an ideal site to study authigenic zeolite and clay mineral assemblages formed by alteration of volcanic ash because: (1) the study is grounded in a long history of zeolite-related research at Olduvai; (2) the co-existence of clay and zeolite minerals has already been established (*e.g.* Hay and Kyser, 2001; Hover and Ashley, 2003; McHenry, 2009); and (3) a single, altered volcanic ash, Tuff IF, can be traced or uniquely identified across a range of diagenetic environments (McHenry, 2005; McHenry *et al.*, 2008; McHenry, in press), providing a known and nearly uniform starting composition.

The objectives of the current study were: (1) to determine the distribution of major and minor elements among coexisting authigenic clay minerals and zeolites in altered tephra at Olduvai; (2) to compare this distribution to the bulk and fresh composition of Tuff IF; and (3) to relate this more broadly to clay mineral and zeolite authigenesis in closed-basin, saline-alkaline lacustrine deposits.

BACKGROUND

Geology of Olduvai Gorge

Modern Olduvai Gorge cuts through the Pliocene-Pleistocene deposits of the Olduvai basin, exposing a transect across an ancient saline-alkaline lake deposit from center to margin. Lacustrine deposits of the Olduvai basin are abundant in Beds I and II, the oldest and thickest units of the Olduvai Formation (Hay, 1976). This lake persisted from ~1.9 to 1.7 Ma (Hay, 1976; Hay and Kyser, 2001). Paleo-lake Olduvai was a closed-basin, saline-alkaline lake that expanded and contracted in response to changes in climate, tectonics, and volcanic input. At times the lake was nearly desiccated,

while at other times it expanded to cover much of the depositional basin with lacustrine sediments (Hay, 1976).

Tephra, derived from the nearby NVH (Figure 1), were deposited within the lake basin. Trachytic compositions dominate the Upper Bed I volcanic record. Tuff IF, the uppermost tephra within Bed I, is the focus of the current study. It is phonolitic (McHenry, 2005), 1.79 Ma in age (Hay and Kyser, 2001), and varies in thickness from 45 cm to 1.5 m within the part of the basin considered in this study. It consists of multiple lava-fragment-rich surge units interspersed with lapilli-rich layers, one of which is widely distributed with lapilli as large as 2 cm in diameter (McHenry *et al.*, 2008; Stollhofen *et al.*, 2008).

The Olduvai tephra were altered within the saline-alkaline lake and associated groundwater, yielding a classic 'bull's-eye' distribution pattern of authigenic phases. The greatest degrees of alteration are at the center (phillipsite + K-feldspar) and the smallest degrees are at the margin (smectite with minor zeolite) (Hay, 1970; McHenry, 2009).

Tephra alteration in closed-basin, saline-alkaline lake environments

The alteration of volcanic materials often leads to saline-alkaline conditions, as Na^+ and K^+ are leached from the glass and as hydrolysis by carbonic acid leads to increased alkalinity (*e.g.* Langella, 2001). Clay minerals form during the early stages of alteration, often as coatings on the altered glass (*e.g.* Snellings *et al.*, 2008). In contact with saline-alkaline fluids, volcanic materials, especially reactive volcanic glass, can alter rapidly to zeolites (*e.g.* Hay, 1966). This can occur as a dissolution-precipitation process, potentially involving a gel phase (Taylor and Surdam, 1981; Sheppard and Hay, 2001), or through neoformation from sufficiently saline and alkaline fluids. The zeolite assemblage formed during alteration will depend on the composition of the starting material and the conditions of diagenesis, including the composition of the diagenetic fluid.

In all cases, minerals other than zeolites also form. Higher pH favors zeolite and authigenic feldspar formation over clay mineral formation, but clay minerals can persist metastably even under more extreme saline-alkaline conditions. Zeolites do not easily accommodate certain elements that are present and often abundant in volcanic glasses (Fe, Mg, Mn, Ti, *etc.*) and these elements are often concentrated in accessory phases instead, including clay minerals and hydroxides.

In a closed-basin lacustrine environment, newly formed zeolites can remain in contact with vestiges of earlier-formed clay minerals and other zeolites. This leaves a textural and mineralogical history of diagenesis that would not always be preserved in an open-system environment where cations excluded from the later-formed zeolites can be more easily removed from the system, or where zeolites crystallize from diagenetic fluids that were formed by leaching elsewhere (Sheppard and Hay, 2001).

METHODS

Sampling and site selection

Sites where Tuff IF had been previously identified (Hay, 1976; McHenry, 2004; McHenry *et al.*, 2008; McHenry, in press) representing a variety of depositional and diagenetic environments (Hay, 1976; McHenry, 2009) were selected for sampling (Figure 2). Within Tuff IF, a widespread lapilli-rich layer (Stolhoffen *et al.*, 2008; McHenry, 2009) was sampled preferentially. Individual lapilli were extracted from the outcrop, and additional pieces of that layer (with both lapilli and matrix) were also collected. Of the twenty samples collected (McHenry, 2009), fifteen were selected for more detailed analysis.

Sample preparation and X-ray diffraction (XRD)

Where possible, individual lapilli were hand-separated, and surface contamination was removed using a picking tool. For samples 08-T35 and 08-T51, individual lapilli could not be extracted and thus a bulk sample of the crystal-poor, lapilli-rich layer was prepared instead. Lapilli separates were then powdered by mortar and pestle. One portion of each powdered sample was mounted in a cavity mount for random powder XRD analysis. Samples were analyzed using a Bruker D8 Focus XRD system (CuKα radiation, 4 s per 0.01º2θ, over the range 2−60º2θ, Sol-X energy dispersive detector) following the methods of McHenry (2009).

The <2 μm size fraction was separated from four samples, limited by sample size. This size fraction was separated from 10 g of the lapilli-rich layer (but not a lapilli separate, as the amount of material was insufficient) by centrifugation and flocculation using $CaCl_2$ following the methods suggested by Moore and Reynolds (1997). These were mounted on glass slides and analyzed both air dried (AD) and ethylene-glycol (EG) saturated using the same instrument (1 s per 0.02º2θ, over the range 2−32º2θ). A portion of each clay separate was also mounted as a random powder and analyzed for its 060 peak using the same instrument (4 s per 0.02º2θ, over the range 58−63º2θ).

X-ray fluorescence (XRF)

Another split of the powdered lapilli was dried overnight at 105ºC and prepared for XRF analysis. One gram of each powder was mixed with ~1 g of ammonium nitrate (oxidizer) and 10 g of a 50:50 lithium metaborate: lithium tetraborate flux, with 1% LiBr as a non-wetting agent. These mixtures were fused at ~1050ºC in a Claisse M4 fluxer to make fused beads. Each bead was analyzed for major, minor, and some trace elements

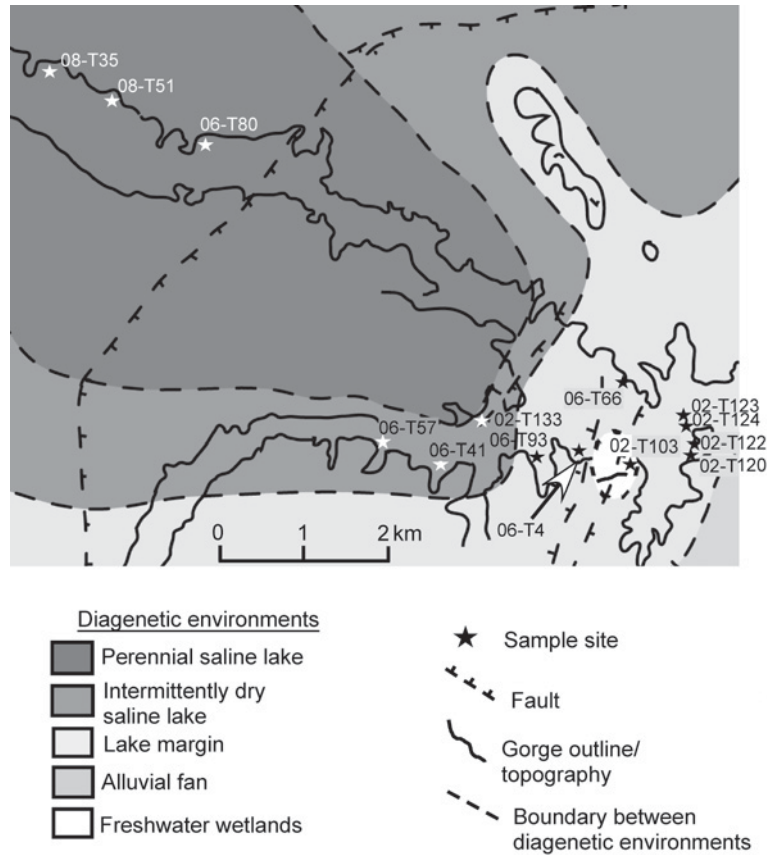

Figure 2. Map of sample locations, including their depositional environments: geography and paleoenvironmental reconstruction after Hay (1976) and Ashley and Hay (2002).

using a Bruker S4 Pioneer XRF, along with USGS rock standards for comparison. A calibration curve was created using eleven USGS igneous and sedimentary rock standards covering a range of compositions, prepared using the same method as the unknowns. Loss on Ignition (LOI) was determined by heating ~1 g of each sample in a muffle furnace at 1050ºC for 15 min. More detailed methods, including information on errors and reproducibility, are available in McHenry (2009).

Electron probe microanalysis (EPMA)

Thin sections of selected samples were prepared, polished, and carbon coated for EPMA. Samples were analyzed at the University of Wisconsin-Madison using a Cameca SX-50 operated at 15 kV and 6 nA with a defocused beam. Na-rich zeolites exhibiting significant Na-loss under the electron beam (a common problem for zeolite analysis, *e.g.* Broxton *et al.*, 1987; Sheppard *et al.*, 1988; Pe-Piper and Tsolis-Katagas, 1991; Chipera *et al.*, 2008) were analyzed using a volatile correction routine, in which the 20 s analysis time was broken down into 4 s intervals (Donovan, 2000). In many samples, the small grain size (<5 μm) of the zeolites and clay-rich coatings made obtaining quantitative compositional information difficult. Thus, many analyses represent crystal clusters rather than individual crystals, and may have low totals because of the void space between adjacent crystals. Clay mineral analyses in particular probably represent an average of multiple adjacent crystals. Phases were initially identified using qualitative Energy Dispersive X-ray Spectrometry (EDS), contrasting backscattered electron (BSE) brightness, and morphology. Phase identification was confirmed using quantitative WDS compositional analysis. Calibration was based on widely available mineral and glass standards, analyzed during the same session.

The quality of the zeolite analyses was determined by calculating a balance error *E*, following the methods of Passaglia (1970):

$$E = 100 \times \frac{(\mathrm{Al} + \mathrm{Fe}^{3+}) - (\mathrm{Na} + \mathrm{K} + 2\mathrm{Ca} + 2\mathrm{Mg} + 2\mathrm{Sr} + 2\mathrm{Ba})}{(\mathrm{Na} + \mathrm{K} + 2\mathrm{Ca} + 2\mathrm{Mg} + 2\mathrm{Sr} + 2\mathrm{Ba})} \quad (1)$$

where all elements are reported in atoms per formula unit (a.p.f.u.). Individual analyses with *E* values >12% were excluded from further consideration and samples with large *E* values overall were re-analyzed using the volatile correction routine.

Scanning electron microscopy (SEM)

Unpolished chips of representative samples were examined using an Hitachi S-8400 scanning electron microscope to observe the crystal shapes and textural relationships between the authigenic minerals. Minerals were identified using their morphology (observed using secondary electron (SE) imaging), the expected assemblage (based on existing XRD data), and EDS. Representative SE images were taken to illustrate the most important textural relationships. Thin sections were also analyzed to obtain high-quality, high-magnification BSE images of the mineral associations.

RESULTS

The XRF and bulk XRD results for most samples were reported by McHenry (2009), which explores the bulk-scale changes in composition resulting from diagenesis. The current manuscript focuses on the EPMA and SEM results, which provide information about the behavior of individual phases during alteration. Bulk XRD results (Table 1, Figure 3) reveal assemblages ranging from nearly fresh glass in the freshwater wetlands environment, some clay minerals in the distal lake margin, to clay minerals and zeolite (chabazite, phillipsite, analcime, or a combination) in the lake margin, and phillipsite with authigenic K-feldspar in the lake center. All altered samples contained at least a small amount of clay minerals. The two new samples (08-T35 and 08-T51) were, unfortunately, not pure lapilli separates, as is indicated by their abundance of volcanic anorthoclase. Bulk compositions (Table 2) revealed a variable but generally Na- and K-rich altered volcanic composition with some mobility for most elements (McHenry, 2009).

The XRD analyses of the <2 μm size fraction revealed that smectite minerals dominate the smaller size fraction. Samples 02-T122 (distal margin), 06-T4 (proximal margin), 06-T41 (intermittently dry), and 06-T80 (central basin) all show significant changes in the 5−10º2θ range between the air-dried and glycolated patterns (Figure 4), though other clay peaks were less pronounced, making the identification of the specific clay mineral phases difficult. The d_{060} values ranged from 1.518 Å (06-T4) to 1.500 Å (02-T122) (Table 1), consistent with dioctahedral smectite compositions (*e.g.* montmorillonite, glauconite/celadonite, Fe-rich smectite) though trioctahedral saponite cannot be ruled out for sample 06-T4 (Moore and Reynolds, 1997).

The EPMA and SEM observations confirmed the presence or absence of volcanic glass detected in the XRD data (Figure 5a,b), and helped establish the textural relationship between coexisting clay minerals and zeolites (Figure 5b−f). In addition, the quantitative WDS data (Tables 3, 4) provide compositions for the authigenic phases, providing a means of determining where, within the assemblage, each element is concentrated.

While the XRD data for many individual samples indicated the presence of multiple zeolites, multiple, distinct EPMA compositions were not observed in most samples. Most zeolitic samples had a single Na- and K-rich zeolite composition, despite differences in morphology and multiple zeolites observed in their XRD patterns. Analcime is identified definitively in sample 02-T123 based on its Na-rich, K-poor composition and trapezohedral crystal shape as imaged by SEM (Figure 6a). A Na-rich, K-poor phase in sample 06-T4 is also probably analcime (Figure 5d); the Na-rich, K-poor phase in sample 06-T93 (not reported due to high *E* and low totals) is more likely chabazite, however, based on the absence of analcime (and the large abundance of

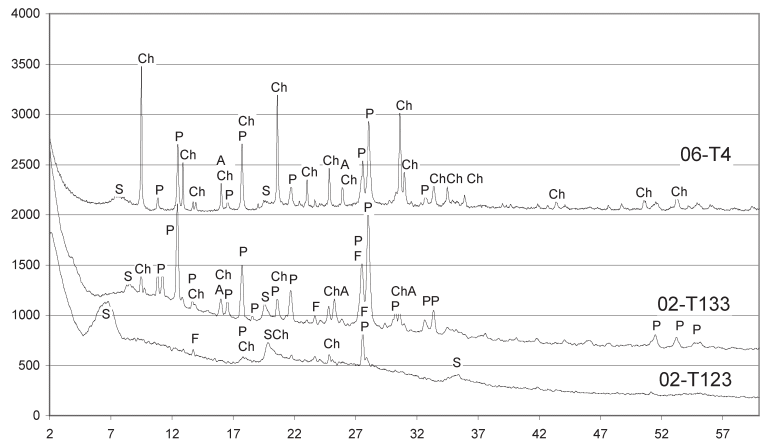

Figure 3. Three representative XRD patterns. Sample 02-T123 is a smectite-rich (S) sample from the distal lake margin with minor zeolite; sample 06-T4 represents the proximal margin with co-existing phillipsite (P), chabazite (Ch), analcime (A), and minor smectite; and sample 02-T133 represents the intermittently dry lake margin and is dominated by phillipsite. Feldspar (F) in this case is a primary volcanic mineral (phenocryst) of anorthoclase composition.

Table 1. Diagenetic environments and authigenic mineral assemblages, from XRD.

Sample	Environment	Max intensity (cps*)	Amorphous	Smectite	Phillipsite	Chabazite	Analcime	Anorthoclase	K-feldspar	Jarosite	Calcite	<2 μm d_{060}
02-T103	Wetland	33	XXX	+	—	—	—	+	—	—	—	
02-T120	Distal margin	180	X	XX	—	+	X	+	—	—	—	
02-T124	Distal margin	115	X	XXX	—	—	X	+	—	—	—	
02-T123 y	Distal margin	142	X	XXX	X	XX	X	+	—	—	—	
02-T123 g	Distal margin	95	XX	XXX	X	X	+	+	—	—	—	
02-T122	Distal margin	145	—	XXX	XXX	XX	XX	+	—	—	—	1.500
06-T66	Proximal margin	175	X	X	XXX	XX	XX	+	—	—	XX	
06-T4	Proximal margin	235	X	X	XXX	XXX	XX	+	—	—	—	
06-T93	Proximal margin	230	—	X	XXX	XXX	—	+	—	—	—	1.518
06-T57	Intermittent	340	X	X	XXX	—	X	+	—	—	—	
06-T41	Intermittent	320	X	XX	XXX	—	X	+	—	—	—	1.513
02-T133	Intermittent	290	—	X	XXX	X	X	+	—	—	—	
06-T80	Lake center	250	—	X	XXX	—	X	+	XX	XX	—	1.511
08-T35	Lake center	340	—	X	XX	—	+	XX	XX	+	—	
08-T51	Lake center	330	—	+	XXX	—	X	XX	XX	X	—	

XXX = abundant. XX = common. X = rare to common. + = rare. – = absent

* Intensity above background of most intense peak

All XRD data from McHenry (2009) except for d_{060} values and 08-T35 and 08-T51, from the present study.

Table 2. Major elements of bulk lapilli separates (XRF), normalized.

Environment	Sample	SiO_2	TiO_2	Al_2O_3	Fe_2O_3	MnO	MgO	CaO	Na_2O	K_2O	P_2O_5	Ba	Zr	LOI	Sum
Wetland	02-T103	62.70	0.67	17.28	6.24	0.20	1.87	1.39	6.18	3.35	0.12	901	620	7.26	99.09
	% error*	0.41	1.44	0.53	0.63	0.87	0.75	0.46	1.13	1.07	1.77	10.00	4.38		
Distal margin/clay dominated															
	02-T124	63.36	0.70	17.19	6.75	0.16	2.13	0.81	6.32	2.50	0.10	864	653	6.62	99.05
	% error	0.41	1.42	0.53	0.61	1.00	0.72	0.56	1.12	1.10	2.05	10.07	4.33		
	02-T123y	62.97	0.58	16.86	6.20	0.13	3.15	0.41	8.24	1.39	0.07	608	725	7.59	94.56
	% error	0.41	1.52	0.53	0.63	1.13	0.67	0.81	1.08	1.16	2.47	11.14	4.31		
	02-T123g	62.69	0.62	17.11	6.69	0.18	2.25	0.73	7.14	2.48	0.09	790	663	6.44	98.96
	% error	0.41	1.47	0.53	0.62	0.91	0.71	0.59	1.10	1.10	2.15	10.25	4.33		
	02-T122	61.15	0.63	17.33	6.60	0.15	3.22	0.23	8.42	2.20	0.06	558	572	7.07	98.50
	% error	0.41	1.48	0.53	0.62	1.04	0.66	1.27	1.08	1.11	2.74	11.22	4.45		
Proximal margin/phillipsite, chabazite															
	06-T66	58.21	0.65	15.94	5.53	0.17	2.07	4.32	10.38	2.65	0.08	939	372	11.67	98.59
	% error	0.42	1.49	0.55	0.66	1.00	0.74	0.35	1.05	1.10	2.44	10.02	4.94		
	06-T4	61.63	0.42	17.68	5.46	0.20	0.66	0.39	10.06	3.45	0.05	482	504	10.07	99.33
	% error	0.41	1.77	0.53	0.65	0.88	1.11	0.84	1.05	1.07	3.01	11.84	4.59		
	06-T93	62.98	0.50	17.68	5.08	0.13	1.25	0.30	9.02	3.03	0.05	459	340	10.06	99.84
	% error	0.41	1.63	0.53	0.66	1.20	0.85	1.03	1.07	1.08	3.54	11.97	5.05		
Intermittent/phillipsite															
	06-T41	61.93	0.56	15.81	5.11	0.07	3.16	0.47	7.41	5.41	0.06	1279	508	7.67	98.73
	% error	0.41	1.55	0.54	0.67	1.77	0.67	0.74	1.10	1.04	2.82	9.36	4.56		
	02-T133	61.19	0.69	16.89	6.25	0.20	1.74	0.64	7.19	5.15	0.06	938	488	7.98	99.24
	% error	0.41	1.44	0.54	0.63	0.89	0.77	0.63	1.10	1.05	2.68	9.91	4.55		
Lake center															
	06-T80	60.80	0.30	16.23	8.14	0.01	0.76	0.18	4.58	8.95	0.06	828	276	9.54	99.51
	% error	0.41	2.07	0.54	0.59	9.79	1.02	1.75	1.20	1.02	3.21	10.30	5.45		
	08-T35	61.68	0.39	15.25	8.61	0.04	1.03	0.36	4.88	7.68	0.09	1584	429	5.61	98.07
	% error	0.42	1.83	0.55	0.59	3.60	0.89	0.81	1.18	1.02	2.70	9.04	4.78		
	08-T51	62.18	0.42	17.30	4.99	0.03	0.58	0.32	6.99	7.12	0.06	909	444	5.76	98.32
	% error	0.42	1.77	0.54	0.67	3.73	1.15	0.86	1.11	1.03	3.57	10.02	4.74		
Fresh glass+															
	02-T103	61.30	0.57	17.76	6.07	0.25	0.50	0.94	8.61	4.49	0.12	n.d.	n.a.		95.65
	St Dev	0.81	0.04	0.26	0.23	0.11	0.04	0.04	0.93	0.26	0.06				1.19

* % error includes the repeatability of the fusion sample preparation method, instrument error, and the counting statistics.
+ EPMA data (average of 27 analyses) from McHenry (2005), normalized to 100%, Fe recalcuated as Fe_2O_3
All results reported as wt.% oxide except for Ba and Zr, reported as ppm
All concentrations normalized to 100% (water-free)
All Fe reported as Fe_2O_3
Sum = pre-normalization sum, including LOI where available
All XRF data previously reported in McHenry (2009) except for errors and samples 08-T35 and 08-T51, from the present study.
n.d. = not detected. n.a. = not analyzed

chabazite) in the XRD patterns and the more rhomb-shaped crystals observed by SEM (Figure 6c–d). Sample 06-T4 was the only sample for which two compositionally distinct zeolites were successfully analyzed by EPMA. The Na-and K-rich zeolite observed in most samples is probably phillipsite, based on its ubiquity in the XRD patterns and its lath shape (Figures 5c–d, 6b–d). Where the lath morphology is absent or uncertain, however, this mineral could be chabazite, which is also identified by XRD in the proximal lake-margin samples (Table 3) and which can have an overlapping compositional range with phillipsite (*e.g.* Sheppard and Hay, 2001).

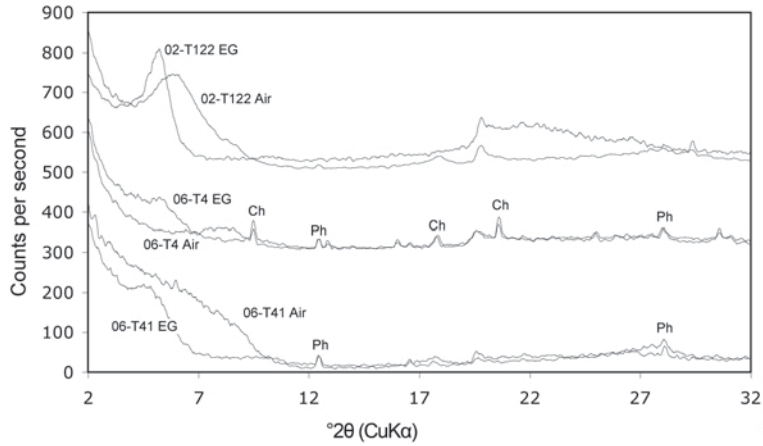

Figure 4. EG-solvated and air-dried (Air) XRD spectra for the <2 μm size fraction of samples 02-T122 (distal margin), 06-T4 (proximal margin), and 06-T41 (intermittently dry). Changes in peak position of 5−10º2θ between the EG and Air samples indicates a significant smectitic component in all three samples. Some fine-grained zeolites are still observed in the <2 μm size fraction.

For clay-mineral analyses, formulae (based on $O_{20}(OH)_4$) and octahedral occupancy were calculated using the EPMA data (Table 4). For most samples the octahedral occupancy is between 3.9 and 4.1 a.p.f.u., indicating that the clay minerals are dioctahedral. This is confirmed by the clay mineral XRD patterns, which show d_{060} values (Table 1) consistent with dioctahedral clays. The most Mg-rich samples had greater octahedral occupancies (4.3−5.0 a.p.f.u.), indicating a trioctahedral component consistent with the greater concentration of divalent cations. Because these octahedral occupancies are intermediate between dioctahedral (4.0 a.p.f.u.) and trioctahedral (6.0 a.p.f.u.), they probably reflect a mixture of clays rather than a single, homogeneous mineral, though a true di-trioctahedral smectite is also possible (*e.g.* Drief and Schiffman, 2004). Low octahedral occupancies for sample 08-T35 (3.75 a.p.f.u.) probably indicate some overlap between clay minerals and zeolites measured by EPMA, especially as this sample appears to be enriched in Na_2O.

The least altered samples analyzed by SEM (02-T120, 02-T123, and 02-T124) still contain volcanic glass, which in places has a thin coating of clay minerals (Figures 5a−b, 6a). Analcime forms rare, larger (2−20 μm) crystals in samples 02-T120 and 02-T123 (round in thin section, trapezohedral in unpolished sample chips, Figures 5b, 6a). More altered samples do not contain glass but retain at least a vestige of the early formed clay coatings, and zeolites crystallized on these clay surfaces. In some samples (*e.g.* 06-T93) these zeolites form thin, void-lining rings, while in other, more altered samples (*e.g.* 06-T41), larger zeolites fill the available space (Figures 5, 6).

DISCUSSION

The authigenic mineral assemblage observed is consistent with previous studies of the Olduvai basin (*e.g.* Hay, 1970; McHenry, 2009). Authigenic K-feldspar is limited to the central basin, where the highest pH and the greatest K^+ activity were probably present. The presence of phillipsite and K-feldspar and the lack of abundant analcime suggests that the diagenetic fluids were low in alkaline earth elements and had a high K^+ activity (Surdam and Eugster, 1976; Chipera and Apps, 2001). Over time, pore fluids were, in general, more dilute (and K^+ activity was lower) further from the lake center, forming phillipsite (but not K-feldspar) in the intermittently dry lacustrine environment, chabazite/phillipsite further out, and clay minerals with only minor zeolites at the distal margins (McHenry, 2009). Smectite is present (at least in small amounts) throughout the basin.

Order of crystallization

Back-scattered electron images of the co-existing clay minerals and zeolites show a consistent pattern. Smectite forms first, forming a thin lining on glass surfaces in the least altered samples (Figure 5a−b). In more altered samples, glass is replaced by smectite, which in some cases preserves the shape of the original glass (Figure 5c). Phillipsite appears to nucleate on these early formed clay surfaces, with laths protruding into the centers of the voids (Figure 5c). As alteration progresses, void space is infilled by additional zeolite crystallization (Figures 5d−e). Analcime crystallization in the least altered (most clay-rich, Figures 5b, 6a) samples definitely post-dated the formation of the clay minerals, but could have happened at a much later time under soil or other conditions independent of the original saline-alkaline lacustrine depositional environment (*e.g* Hay, 1970; Renaut, 1993).

Establishing the order of crystallization of co-existing zeolites is more difficult. In sample 06-T93, phillipsite and chabazite form distinct clusters on the underlying clay substrate and are rarely in direct textural association. This could suggest that the two grew

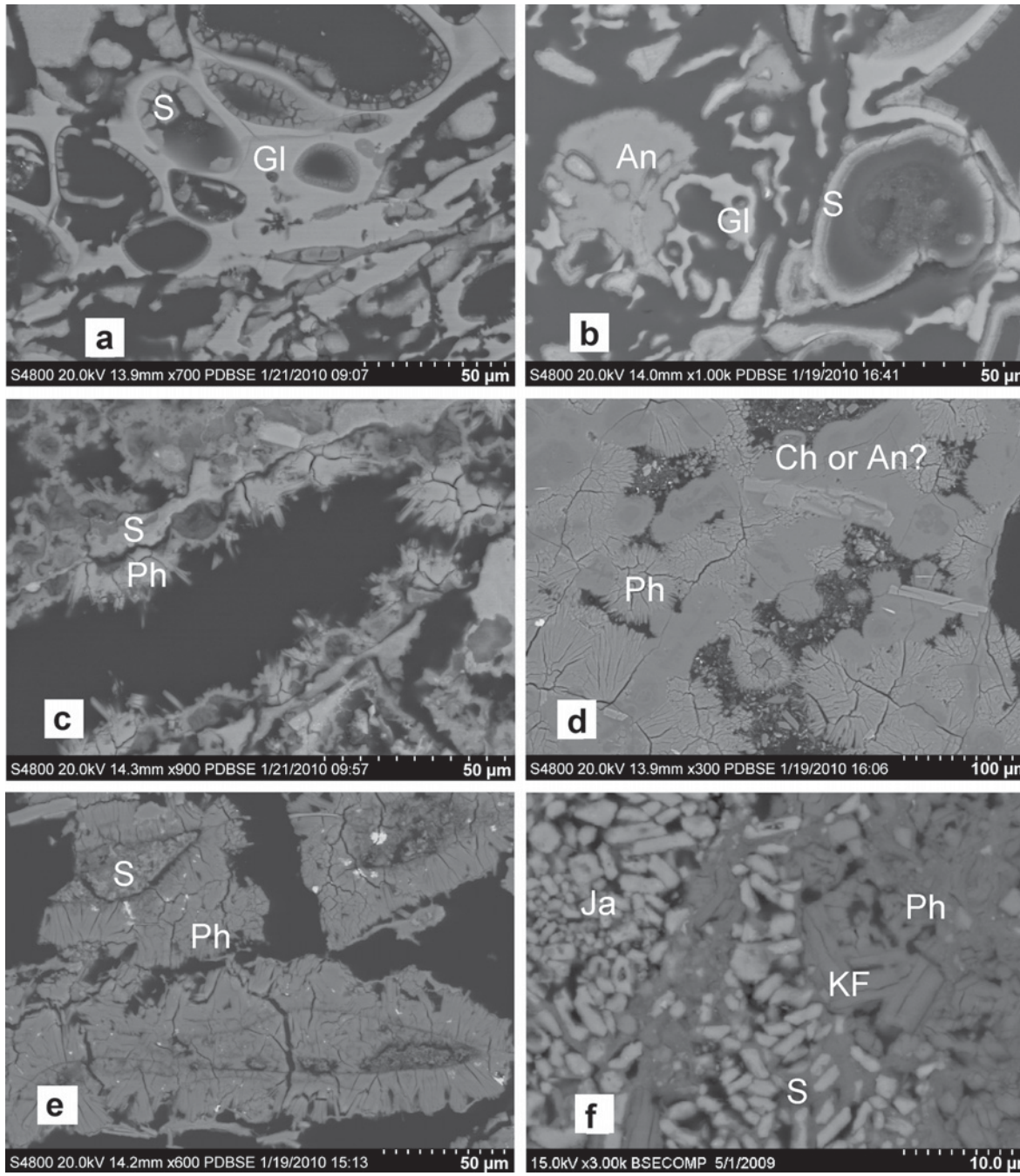

Figure 5. BSE images of samples in thin section. (a) Sample 02-T124, distal lake margin. A thin layer of clay (S) lines the vesicles within the glass (Gl) of a Tuff IF lapillus. (b) Sample 02-T123, distal lake margin. A thin coating of clay lines the vesicles within and replaces degraded volcanic glass. A large, round, Na-rich zeolite (probably analcime: An) appears to grow around the replaced glass. (c) Sample 06-T93, proximal lake margin. Glass is absent, yet clays retain some morphology of the original glass. Phillipsite (Ph) laths appear to nucleate on the clay and grow out into the void. (d) Sample 06-T4, proximal lake margin. Co-existing phillipsite (radiating laths) and a more Na-rich zeolite (analcime or chabazite (Ch): darker, more circular crystals in BSE) fill most of the space. (e) Sample 06-T41, intermittently dry lacustrine. Thick masses of zeolite nucleate on the remaining clay, filling void space. (f) 06-T80, lake center. Phillpsite, authigenic K-feldspar (KF), clay, and jarosite (Ja) co-exist.

simultaneously. In several spots where both are seen in cross-section, however, a thin layer of chabazite appears to underlie clusters of phillipsite laths, suggesting that at least some of the chabazite formed earlier (Figure 6c). No instances of chabazite overgrowing phillipsite were observed, consistent with the observations of Mees *et al.*

Table 3. EPMA analyses of zeolites.

Sample Zeolite *n*	02-T122 Phillip-site 4	02-T123 Anal-cime 10	06-T66 Phillip-site 3	06-T4 P1 Anal-cime 5	06-T4 P2 Phillip-site 5	06-T93 Phillip-site 5	06-T41 Phillip-site 4	06-T57 Phillip-site 4	02-T133 Phillip-site 7	06-T80 Phillip-site 12	08-T35 Phillip-site 13	08-T51 Phillip-site 8
SiO_2	58.69	56.81	60.03	54.45	59.73	61.55	58.09	62.15	60.53	60.10	56.95	57.77
St. dev.	3.88	2.04	2.65	1.95	1.45	0.92	2.83	0.72	1.59	3.40	2.81	2.06
TiO_2	n.d.	0.12	0.02	0.11	0.19	0.03	n.d.	n.d.	0.13	0.00	n.a.	0.3
St. dev.		0.03	0.02	0.07	0.07	0.02			0.12	0.00		0.06
Al_2O_3	19.71	17.28	18.33	18.11	18.90	18.58	16.38	18.37	18.92	16.46	16.07	16.26
St. dev.	2.07	0.40	0.40	0.42	0.33	0.47	1.04	0.54	0.92	0.97	1.04	0.77
Fe_2O_3	0.31	0.39	0.06	0.25	0.27	0.21	0.56	0.19	0.62	0.62	0.92	0.42
St. dev.	0.16	0.10	0.03	0.07	0.14	0.08	0.44	0.09	0.62	0.51	0.64	0.28
MnO	0.00	0.07	0.02	0.03	0.03	0.05	n.d.	n.d	0.01	0.04	0.03	0.07
St. dev.	0.00	0.08	0.03	0.05	0.03	0.03			0.02	0.05	0.04	0.04
MgO	0.01	0.08	0.03	0.02	0.01	0.02	0.38	0.08	0.23	0.15	0.14	0.07
St. dev.	0.01	0.05	0.01	0.02	0.02	0.02	0.00	0.02	0.30	0.15	0.08	0.03
CaO	0.44	0.67	0.02	0.11	0.08	0.01	0.01	0.59	0.07	0.06	0.03	0.05
St. dev.	0.22	0.17	0.02	0.05	0.08	0.01	0.04	0.05	0.03	0.05	0.04	0.01
Na_2O	7.59	8.71	7.71	10.12	6.84	6.54	5.26	4.92	6.05	5.33	6.03	6.09
St. dev.	0.36	0.68	0.22	2.04	0.84	0.49	0.68	0.48	1.43	0.66	0.82	0.45
K_2O	4.12	0.16	3.51	2.50	5.59	5.59	5.16	6.60	6.01	6.10	5.49	5.93
St. dev.	0.82	0.09	0.08	0.53	0.27	0.88	0.30	0.29	0.55	0.23	0.4	0.28
BaO	n.d.	n.d.	0.09	0.08	0.19	0.07	0.09	0.41	n.d.	n.d.	n.a.	n.a.
St. dev.			0.12	0.11	0.21	0.07	0.10	0.32				
Sum	90.85	84.25	89.77	85.74	91.62	92.48	85.66	93.29	92.50	88.80	86.16	86.87
St. dev.	7.14	1.69	3.01	2.23	1.66	1.86	4.23	1.56	2.43	4.45	3.86	3.05
Number of ions on the basis of framework of 32 oxygens (phillipsite) or 96 oxygens (analcime)												
Ox #	32	96	32	96	32	32	32	32	32	32	32	32
Si	11.52	35.39	11.83	34.19	11.67	11.85	12.02	11.92	11.71	12.08	11.88	11.90
Ti	0.00	0.06	0.00	0.05	0.03	0.00	0.00	0.00	0.02	0.00	0.08	0.05
Al	4.56	12.69	4.26	13.40	4.35	4.22	4.00	4.15	4.31	3.90	3.95	4.00
Fe	0.05	0.20	0.01	0.13	0.04	0.03	0.10	0.03	0.10	0.10	0.14	0.13
Mn	0.00	0.04	0.00	0.02	0.00	0.01	0.00	0.00	0.00	0.01	0.01	0.01
Mg	0.00	0.07	0.01	0.02	0.00	0.01	0.12	0.02	0.07	0.04	0.04	0.02
Ca	0.09	0.45	0.00	0.07	0.02	0.00	0.00	0.12	0.01	0.01	0.01	0.01
Na	2.89	10.52	2.95	12.31	2.59	2.44	2.11	1.83	2.27	2.08	2.44	2.44
K	1.04	0.12	0.89	2.02	1.41	1.38	1.37	1.63	1.49	1.58	1.47	1.58
Ba	0.00	0.00	0.01	0.02	0.01	0.01	0.01	0.03	0.00	0.00		
Si/Al	2.53	2.79	2.78	2.55	2.68	2.81	3.01	2.87	2.72	3.10	3.01	3.02
E	10.67	8.69	9.90	−7.90	7.10	9.48	7.06	9.00	9.83	3.39	−1.66	−2.99

E = balancing factor
n = number of analyses averaged, St. dev. = standard deviation
Samples analyzed using a Cameca SX-50 operated at 15 kV and 6 nA with a defocused beam
n.a. = not analyzed, n.d. = not detected
All results presented as wt.% oxide

(2005), and supporting a model in which the pH and K^+ activity of the diagenetic fluids increased over time. Unfortunately, the rarity of unambiguous analcime in samples with other zeolites made determining its relationship to the other zeolites impossible.

Element mobility

Patterns of element mobility for bulk Tuff IF lapilli across the basin were determined by McHenry (2009), and relevant observations are summarized here (Table 2). Al was the least mobile element throughout the basin, and was thus used in the calculation for the isocon line (after Grant, 1986) used in Figure 7. The changes in major-element concentrations between the freshest bulk sample (02-T103) and four altered samples (02-T123, 02-T122, 02-T133, and 06-T80) are displayed graphically in these isocon plots. Such plots are often used to determine the effects and extent of volume loss

Table 4. EPMA analyses of clay minerals.

Sample	02-T124	02-T122	02-T122	02-T123	06-T66	06-T4	06-T4	06-T93	06-T41	06-T41	06-T57	02-T133	06-T80	06-T80	08-T35
Clay	Al-rich	Al-rich	Fe-rich	Al-rich	Fe-rich	Fe-rich		Fe-rich	Fe-rich	Mg-rich		Fe-rich		Fe-rich	
n	18	6	4	22	24	5	5	10	3	3	2	19	8	2	5
SiO_2	57.15	52.44	46.56	55.92	50.64	47.79	52.33	48.52	51.67	54.00	45.23	47.06	50.87	44.26	44.35
St. dev.	2.50	2.49	1.38	2.94	2.41	2.72	1.23	1.91	1.82	1.46	2.91	3.02	2.81	4.99	2.93
TiO_2	0.66	0.83	1.86	0.71	1.37	1.34	0.97	1.04	0.81	0.90	-0.94	1.15	0.21	0.48	0.24
St. dev.	0.08	0.23	0.27	0.18	0.50	0.47	0.10	0.35	0.07	0.36	0.31	0.29	0.09	0.48	0.15
Al_2O_3	15.72	13.55	10.17	14.52	9.04	4.83	8.49	6.20	3.15	4.19	6.10	8.76	10.72	8.33	4.79
St. dev.	1.14	1.05	0.61	1.35	1.37	0.73	0.41	2.09	0.36	0.48	0.36	0.84	1.42	2.28	1.00
Fe_2O_3	7.01	10.08	16.71	9.35	13.90	20.43	9.79	18.06	15.58	6.81	12.13	14.36	13.07	24.19	16.17
St. dev.	1.36	5.80	1.66	2.71	1.70	2.48	2.12	1.83	1.76	1.11	0.59	1.80	3.46	0.91	2.21
MnO	0.02	0.05	0.17	0.05	0.17	0.60	0.14	0.31	0.24	0.08	0.08	0.18	0.01	0.11	n.d.
St. dev.	0.03	0.05	0.12	0.04	0.08	0.06	0.06	0.10	0.05	0.08	0.16	0.07	0.02	0.12	
MgO	3.61	5.06	4.08	4.89	5.12	4.37	8.62	4.71	12.24	19.83	3.59	5.12	1.55	4.30	2.55
St. dev.	1.17	0.29	0.70	1.66	1.13	0.71	1.62	1.03	2.82	1.72	0.02	0.59	0.50	2.67	0.61
CaO	1.38	1.04	0.72	1.34	0.18	0.49	0.27	0.09	0.04	0.07	0.51	0.49	0.05	0.04	0.28
St. dev.	0.56	0.28	0.16	0.44	0.37	0.32	0.10	0.04	0.04	0.02	0.12	0.20	0.04	0.00	0.51
Na_2O	0.63	1.13	0.76	0.66	3.51	2.03	1.74	1.38	2.37	3.22	0.91	0.73	1.80	1.03	2.23
St. dev.	0.16	0.59	0.43	0.40	0.71	0.60	0.40	0.22	0.15	1.20	0.53	0.42	0.48	0.23	0.40
K_2O	0.89	1.87	5.10	1.49	3.24	3.96	3.47	3.98	3.68	2.87	4.31	4.98	5.32	5.86	3.59
St. dev.	0.15	0.09	0.50	0.47	0.57	0.40	0.40	0.91	0.29	0.12	0.07	0.49	1.40	1.40	0.47
BaO	n.d.	0.01	0.01	n.d.	0.12	0.05	0.04	0.15	0.09	0.00	n.a.	0.04	n.d.	n.d.	n.a.
St. dev.		0.02	0.02		0.11	0.08	0.10	0.18	0.16	0.00		0.07			
Sum	86.35	85.06	84.46	88.00	85.83	83.83	84.87	82.61	88.37	91.30	70.60	81.42	82.28	86.15	74.24
St. dev.	2.90	3.30	1.84	4.02	3.34	4.41	2.06	3.66	3.54	2.34	1.57	4.23	3.18	2.55	3.87
Number of ions on the basis of framework of $O_{20}(OH)_4$															
n	18	6	4	22	24	5	5	10	3	3	2	19	8	2	4
O #	22	22	22	22	22	22	22	22	22	22	22	22	22	22	22
Si	7.90	7.57	7.12	7.71	7.50	7.44	7.71	7.56	7.53	7.47	7.80	7.41	7.81	6.83	7.72
Ti	0.07	0.09	0.21	0.07	0.15	0.16	0.11	0.12	0.09	0.09	0.13	0.14	0.02	0.06	0.03
Al	2.56	2.30	1.83	2.36	1.58	0.89	1.47	1.14	0.54	0.68	1.30	1.62	1.94	1.52	0.98
Fe	0.73	1.09	1.92	0.97	1.55	2.39	1.09	2.12	1.71	0.71	1.65	1.70	1.51	2.81	2.36
Mn	0.00	0.01	0.02	0.01	0.02	0.08	0.02	0.04	0.03	0.01	0.01	0.02	0.00	0.01	0.00
Mg	0.74	1.09	0.93	1.01	1.13	1.02	1.89	1.09	2.66	4.09	0.96	1.20	0.35	0.99	0.66
Ca	0.20	0.16	0.12	0.20	0.03	0.08	0.04	0.01	0.01	0.01	0.10	0.08	0.01	0.01	0.05
Na	0.17	0.32	0.23	0.18	1.01	0.61	0.50	0.42	0.67	0.86	0.32	0.22	0.54	0.31	0.75
K	0.16	0.35	1.00	0.26	0.62	0.79	0.66	0.80	0.69	0.51	1.00	1.01	1.05	1.16	0.80
Ba	0.00	0.00	0.00	0.00	0.01	0.00	0.00	0.01	0.01	0.00		0.00	0.00	0.00	
Oct Al	2.56	1.87	0.96	2.07	1.08	0.33	1.18	0.69	0.07	0.15	1.10	1.03	1.94	0.34	0.70
Oct T	4.11	4.15	4.05	4.13	3.93	3.97	4.28	4.07	4.56	5.05	3.85	4.09	3.83	4.21	3.75
Int	0.73	0.99	1.47	0.84	1.68	1.57	1.24	1.24	1.37	1.39	1.42	1.40	1.60	1.48	1.61

Oct Al: Octahedral aluminum. Oct T: Octahedral total. Int: interlayer cations
n = number of analyses averaged, St. dev. = standard deviation, n.a. = not analyzed; n.d. = not detected.
Samples analyzed using a Cameca SX-50 operated at 15 kV and 6 nA with a defocused beam
All results presented as wt.% oxide

during weathering and soil formation, but this is difficult or impossible without knowing the density before and after (*e.g.* Grant, 2005). Nevertheless, isocon plots calculated without density can still be used to show relative enrichments and depletions of mobile elements relative to fresher compositions (*e.g.* Franzson *et al.*, 2008).

SiO_2 and Fe_2O_3 lie close to the isocon line for all four samples, indicating that their concentrations are relatively unchanged by alteration. Na_2O also varies little, with slight enrichment in the distal margin samples and depletion in the central basin. MgO increases in the distal margin samples (probably reflecting the formation of abundant Mg-rich smectites)

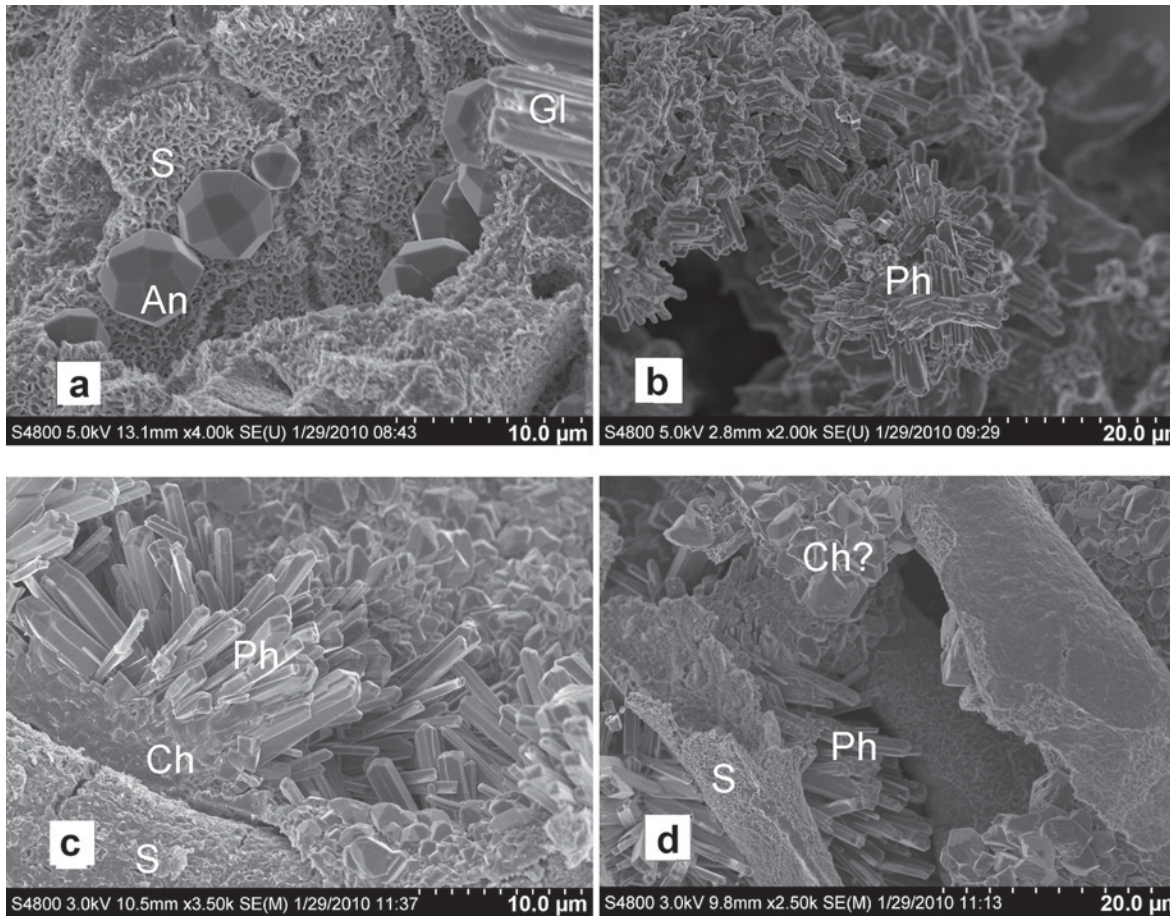

Figure 6. SE images of sample chips. (a) Sample 02-T120, distal lake margin. Large, euhedral analcime (An) crystals grow on a substrate of smectite (S). Volcanic glass (Gl) is visible in the upper right hand corner. (b) Sample 06-T41, intermittently dry lacustrine. Abundant phillipsite (Ph) laths. (c) Sample 06-T93, proximal lake margin. Phillipsite, chabazite (Ch), and smectite. Phillipsite laths appear to grow on a thin layer of chabazite crystals that overgrow smectite. (d) Sample 06-T93, proximal lake margin. Phillipsite and chabazite clusters associated with smectite-replaced volcanic glass.

but decreases in the sample from the central basin (06-T80). P_2O_5 and CaO decrease in all four altered samples. K_2O appears to be conserved in the distal margin samples (02-T122 and 02-T123) and enriched in the intermittently dry and central basin samples (02-T133, 06-T80), a trend consistent with the crystallization of abundant phillipsite and authigenic K-feldspar. All three of the central lake basin samples (06-T80, 08-T35, and 08-T51) show this enrichment in K_2O accompanied by a phillipsite and authigenic K-feldspar-rich mineral assemblage. These trends are discussed in more detail in McHenry (2009). Despite the observed mobility during alteration, these changes are much less than would be expected in an open-system environment. Most mobile elements are conserved (though redistributed) within the system. Under open-system conditions, removal of leached cations could lead to significant changes in bulk composition or zeolites could form from solution far from the area where glass alteration occurred.

Element partitioning between clays and zeolites

The relative constancy of the bulk composition despite significant differences in diagenetic conditions and authigenic mineral assemblages can be explained in part by the partitioning of elements between the co-existing phases. For example, where clay minerals are a minor constituent compared to zeolite, their compositions must be more Fe-rich than clay minerals from more dilute environments to accommodate the Fe in the sample, assuming that they are the only significant repository for Fe. Using the compositions of the co-existing clay minerals and zeolites and the original glass composition (holding Al constant), the relative abundances of the two phases can be estimated. Deviations from this model show the effects of element mobility beyond the centimeter scale and potential contributions from other phases.

To determine the partitioning of elements from the glass between co-existing zeolite and clay phases, the

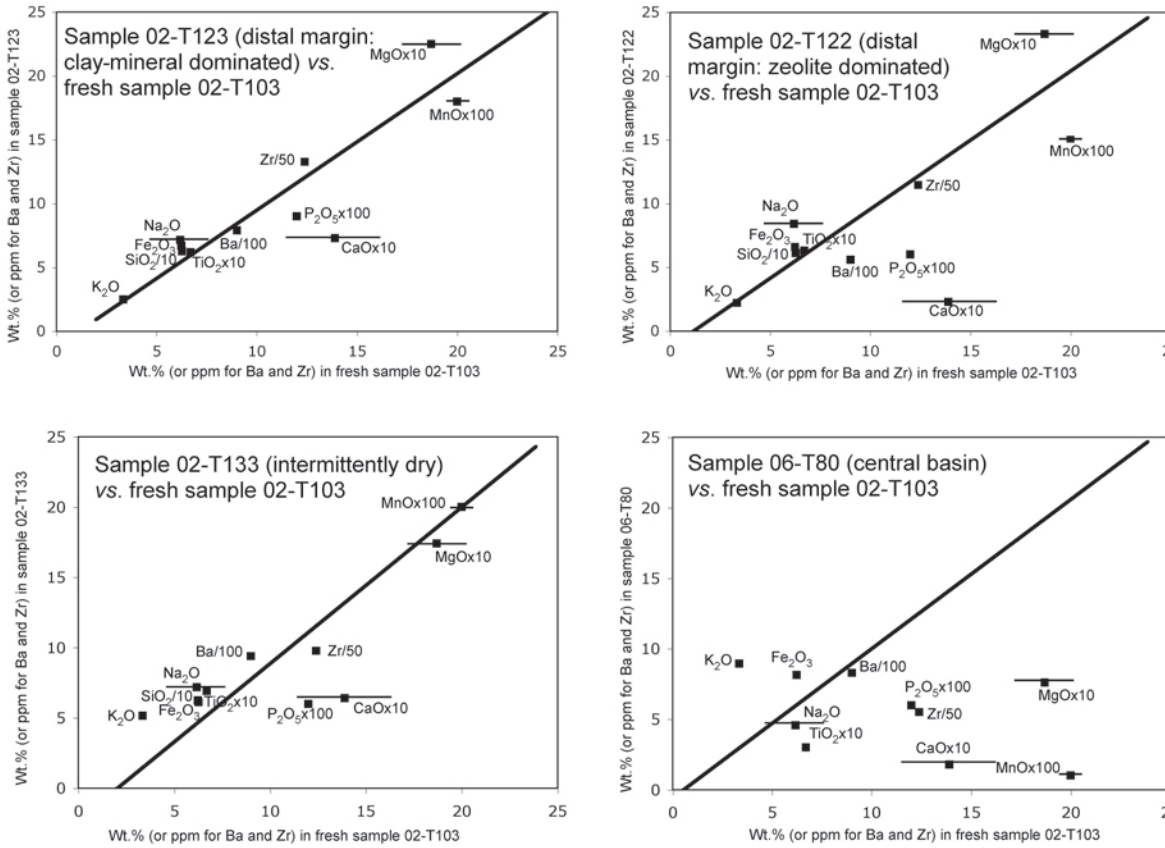

Figure 7. Isocon diagrams, showing the enrichment or depletion of major and minor elements between the least altered bulk sample (02-T103) and four representative altered samples. The isocon line was calculated using a combination of Al_2O_3 and trace elements Hf, Th, and Ta (concentrations from McHenry, 2009) for samples 02-T123, 02-T122, and 02-T133, and Al_2O_3 and SiO_2 for sample 06-T80. Each point represents the concentration of a single element in the altered sample plotted against sample 02-T103. To observe all of these elements at the same scale, a multiplier (indicated next to each symbol) is used. The error bars represent the standard deviation of the composition of the three freshest bulk samples reported in McHenry (2009), showing the observed variation within the freshest samples. Where no error bar is shown, the standard deviation is smaller than the size of the symbol. Elements showing enrichment plot above the isocon line, elements showing depletion plot below.

EPMA results for the fresh glass and the clay minerals and zeolites from four samples (02-T123, 02-T133, 06-T66, and 06-T93) were normalized to 100% and used to make a mixing model. McHenry (2009) demonstrated that Al_2O_3 was the least mobile element during both zeolitic and argillic alteration within Tuff IF at Olduvai, and thus was chosen for normalization. Assuming that the alteration of the original volcanic glass is the source of all Al_2O_3 for both the zeolite and clay, and that the zeolite and clay compositions analyzed represent the only significant alteration products, the relative percentages in each sample can be determined using the following equation:

$$Al_Z + (1 - Al_C) = Al_G \quad (2)$$

where Al is the Al_2O_3 concentration (EPMA analyses normalized to 100%) for the zeolite (Z), clay mineral (C), and glass (G) components. Using these percentages, one can determine which elements are accounted for by *in situ* partitioning of glass components between coexisting clay minerals and zeolites, and which are not. This approach was only taken with samples that contained a single zeolite composition (as successfully analyzed by EPMA), a single clay-mineral composition, and no authigenic feldspar to keep the model simple.

The results of these calculations (shown in Table 5) mirror the XRD results, with zeolites being a smaller part (34%) of clay-dominated sample 02-T123 from the distal lake margin. Samples 06-T66, 06-T93, and 02-T133 from the proximal margin and intermittently dry lake range from 73 to 81% zeolite according to these calculations.

The same approach can be used holding elements other than Al constant, and this can provide insight into their relative mobility in the different environments. For example, recalculations involving Ti instead of Al produce the same result for the least altered sample (02-T123) but overestimate the abundance of clay

Table 5. Predicted glass composition (wt.%) based on mixtures of clay minerals and zeolite as estimated by Al_2O_3 content.

Sample	SiO_2	TiO_2	Al_2O_3	Fe_2O_3	MnO	MgO	CaO	Na_2O	K_2O	BaO	Sum
02-T103											
Actual glass composition, as measured by EPMA (McHenry, 2005), n = 21											
	61.30	0.58	17.76	5.46	0.25	0.49	0.94	8.62	4.49	0.12	100.00
02-T123											
Predicted original glass composition based on 34% zeolite, 66% clay											
	64.42	0.58	17.76	7.08	0.07	3.64	1.26	4.03	1.17		100.00
06-T66											
Predicted original glass composition based on 73% zeolite, 27% clay											
	64.34	0.45	17.76	4.36	0.06	1.62	0.06	7.50	3.75	0.10	100.00
06-T93											
Predicted original glass composition based on 81% zeolite, 19% clay											
	64.35	0.23	17.76	4.26	0.07	1.04	0.03	6.82	5.35	0.08	100.00
02-T133											
Predicted original glass composition based on 73% zeolite, 27% clay											
	63.05	0.48	17.76	5.19	0.07	1.86	0.21	5.00	6.36	0.01	100.00

Percentages of zeolite and clay are based on the observation that Al_2O_3 is conserved during alteration (McHenry, 2009) and the simplifying assumption that it is redistributed between only two phases: one clay mineral and one zeolite.
Deviations from the actual glass composition for individual elements indicate the effects of leaching, enrichment, or partitioning into additional, unanalyzed phases.

minerals in zeolitic samples. This can be explained by the apparent net loss of TiO_2 during zeolitic alteration as observed by McHenry (2009).

Using the estimated percentages of zeolite and clay minerals in each of the samples, one can predict the composition of the original glass (Table 5). A comparison between the predicted and actual glass composition clearly reveals which elements were conserved and which are concentrated or lost. Elements that appear to stay within the system include Al and Fe. When normalized to Al_2O_3, the modeled bulk composition is slightly higher in SiO_2 than the original glass. This helps explain the lack of opal-CT or another Si-rich alteration product (common constituents of zeolitically altered rhyolites, *e.g.* Boles and Coombs, 1975). With the starting phonolitic composition, the Si concentration is insufficient to form these Si-rich phases.

K_2O appears to have been leached from the less altered samples (02-T123 and 06-T66) and concentrated in the more altered samples (02-T133 and 06-T93), an observation consistent with the XRF results and the appearance of K-bearing phillipsite as the dominant phase in the more altered samples. MgO is concentrated in most samples, but especially in the most clay-rich sample (02-T123), and is probably attributable to the formation of Mg-bearing smectite. Mg for smectite formation was probably available in groundwater that had previously leached basalts in the nearby NVH (McHenry, 2009), and tends to become concentrated in saline-alkaline lake waters (*e.g.* Jones and Weir, 1983; Jones and Deocampo, 2003).

When clay minerals become a minor component of the assemblage (as in samples 02-T133, 06-T66, and 06-T93), they become more concentrated in the components of the original glass that are not easily accommodated by the zeolites, such as Fe, Mg, and Ti. For example, zeolite-poor sample 02-T123 clay has 0.8% TiO_2 (normalized), while 02-T133 clay has 1.4%, 06-T66 clay has 1.57%, and 06-T93 clay has 1.23%. Thus, a smaller amount of clay is required to accommodate the Ti from the glass. Clay minerals remain predominantly dioctahedral, with additional Fe(III) in place of Al in the octahedral sheets. A net loss of Ti during zeolitization (McHenry, 2009) could also contribute to this trend. Similarly, the concentration of Al in the clay minerals is significantly less in the zeolite-rich samples than in the clay-rich samples (Figure 8). Three possible explanations for this observation are: (1) the smaller Al concentration is required to accommodate the increased Fe and Mg content in the clay minerals; (2) more Al is needed for the more abundant, Al-rich zeolites (because the concentration of Al remains unchanged overall); (3) clays with a large Mg/Al ratio are favored by the more saline, alkaline water of the central basin (*e.g.* Deocampo *et al.*, 2002).

Note that a simple mixture of the zeolite and clay compositions measured in the proportions estimated using this approach does not yield the composition of the bulk samples as determined by XRF (Table 2). Sample 02-T123 still contains relict glass, which complicates the mixing model. CaO is underestimated (especially for sample 06-T66, which contains calcite) and Na_2O is underestimated for all samples, indicating that Na_2O may be held by another phase, or that more Na was lost during EPMA analysis of the zeolites than was lost during analysis of the glass. In the case of sample 06-T93, an unsuccessfully analyzed Na-rich zeolite

(probably chabazite, based on the XRD pattern) could not be incorporated into the model. This omission would be unlikely to change the relative percentages of clay and zeolite in the mixing model, assuming that this zeolite has a similar Al_2O_3 concentration compared to the Na-rich zeolites analyzed successfully in samples 02-T123 and 06-T4 (where the Na- and K-rich zeolites have similar Al_2O_3 concentrations), but could account for the underestimation of Na for this sample. Mn oxides were observed qualitatively in some samples, and could house the missing MnO. Phenocrysts make up a small proportion of the lapilli-rich layer of Tuff IF, and thus probably do not contribute significantly to the bulk composition (McHenry, 2009). Detrital contamination does not play a significant role in the mineral assemblage, because the lapilli layer of Tuff IF is enclosed by the Tuff IF surges.

Formation model

The volcanic glass was the main source of the elements present in both the zeolites and clay minerals. The initial stage of tephra alteration in contact with ground and surface water involved the liberation of Na^+ and K^+ during hydrolysis of the glass, increasing the salinity and alkalinity of the fluids. Clay minerals formed, adhering to and replacing the glass surfaces. The overall Mg content increased during this stage, brought in by Mg-enriched fluids from weathering in the nearby NVH and allowed by the saline-alkaline lake water to become concentrated. In the lake-margin environment, alteration stopped at this point, retaining some glass. Analcime formed at some point after the clays, but whether this occurred immediately after clay formation or more recently is uncertain.

Within the pore fluids of the lake-margin region, salinity and alkalinity fluctuated with lake level, allowing chabazite and phillipsite to nucleate on the clay surfaces, filling the void spaces between and within the lapilli. In the lake margins this coating remains thin, while in the intermittently dry lacustrine samples the interstices are more filled in by zeolite growth, either the result of neoformation of zeolite in the more saline-alkaline fluids or continued degradation of the original glass. The zeolites did not replace the glass directly, but were probably precipitated from solution. The remaining clays contain less Al and are (in general) more concentrated in Mg, Ti, and Fe compared to those from the distal margin (Figure 8), whereas the concentration of K relative to Na in the Na- and K-rich zeolites increases with proximity to the lake center (Figure 9). The pH was highest and the K^+ activity greatest in the central lake basin, where K-feldspar replaced phillipsite (McHenry, 2009). The replacement of phillipsite by K-feldspar probably took tens of thousands of years (*e.g.* Hay and Guldman, 1987), and indicates that pore waters

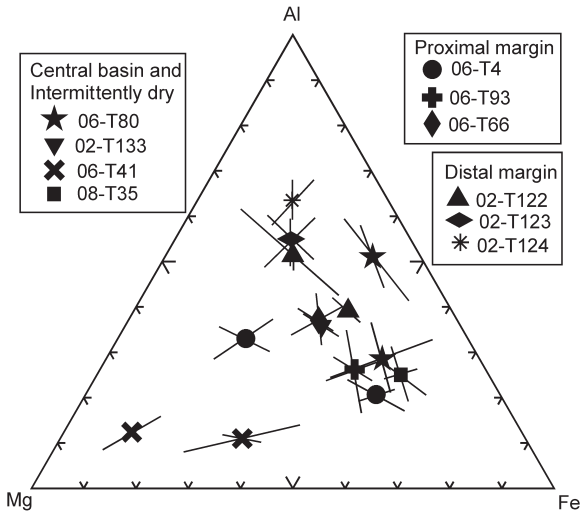

Figure 8. Ternary diagram showing the relative Mg, Al, and Fe contents of the average composition clay mineral (based on formula units) for each sample (see Table 4 for values of *n*). Some samples had more than one clay mineral composition, in which case both are plotted (with the same symbol). One standard deviation for each element is plotted as a line that would intersect the appropriate apex. Where no standard deviation is plotted, it was not substantially larger than the size of the symbol. The samples from the distal margin (where zeolitization is minimal) tend to have the greatest relative Al contents in their clays. The most zeolitized samples are more Fe-rich than Al- or Mg-rich, with the notable exception of sample 06-T41, which has Mg-rich clays.

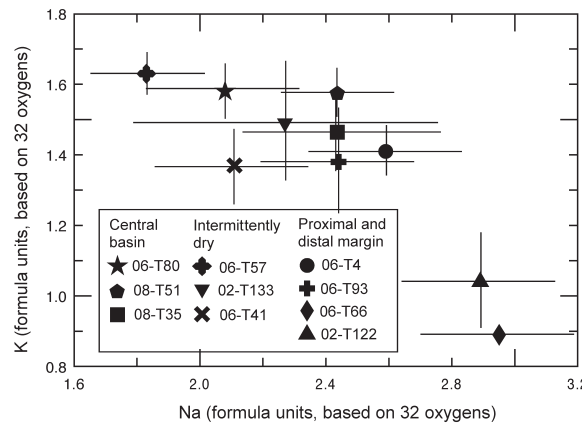

Figure 9. Na *vs*. K for Na- and K-rich zeolites. Analcime was excluded from consideration. A bivariate plot was selected over a ternary plot because Ca is close to zero for all samples. Formula units (based on 32 oxygens) were used to minimize the influence of hydration. Error bars for each sample are plotted for one standard deviation from the average value reported (see Table 3 for values of *n*) and show that analyses were more variable for Na than for K. Samples from the central lake basin and intermittently dry lacustrine environments show smaller Na and greater K concentrations, while samples 02-T122 and 06-T66 from the proximal and distal margin show the opposite trend. Thus, the general trend is toward more K-rich zeolites near the basin center and more Na-rich zeolites farther out.

remained saline-alkaline long after the lake itself dried up. Between the coexisting zeolites and clays, the original glass composition was largely retained.

Other lake basins

The trends described are probably applicable to marginal lake facies and adjacent alluvial deposits in other closed-system saline-alkaline environments, where early formed minerals (such as smectite) are retained during subsequent alteration events. Without a significant flux of cations entering or leaving the system, the overall bulk composition changes little and the Na-, K-, and Ca-bearing zeolites must be accompanied by Fe-, Mg-, and Ti-bearing clay minerals. As zeolites become a larger part of the overall assemblage, the accompanying clay minerals change to accommodate these changes (Al rich to Mg and/or Fe rich). Other closed-basin zeolite deposits with coexisting clay minerals and zeolites include the Miocene clinoptilolite tuffs of the central Simav graben, Turkey (Snellings *et al.*, 2008); Lake Tecopa, California (Sheppard and Gude, 1968; Larsen, 2008); the Big Sandy Formation, Arizona (Sheppard and Gude, 1973); and others. Smectite and zeolites also coexist in non-lacustrine closed-system, saline-alkaline settings, including the altered Tertiary silicic volcanic rocks beneath Pahute Mesa in the Nevada Test Site (Moncure *et al.*, 1981), and might follow similar compositional trends. Close examination of the compositions of co-existing clay minerals and zeolites from these or other similar sites could help test whether this pattern of element partitioning between authigenic phases is generally applicable, or unique to Olduvai.

CONCLUSIONS

Clay minerals are ubiquitous in tephra altered under saline-alkaline lacustrine conditions from Olduvai Gorge, Tanzania, even where zeolites are the dominant authigenic minerals. In a closed system, early-formed minerals (such as smectite) can remain in the system long after diagenetic conditions change. These clays become a repository for those elements that were present in the original volcanic glass but which are excluded from the structure of the later-formed zeolites, such as Ti, Mg, and Fe. These elements became even more concentrated in the clay minerals when the clay minerals are a minor component of the assemblage, helping to retain the overall bulk composition of the deposit.

Within the altered Olduvai tephra, most compositional changes can be accounted for by a redistribution of elements present within the glass and the authigenic zeolite and clay minerals. Only Mg requires an external source. Leaching of K^+ during hydrolysis of glass in the more dilute lake margin can account for greater concentrations of K_2O in the central basin. Olduvai is thus a good example of conservation of initial composition during closed-system zeolitic diagenesis.

ACKNOWLEDGMENTS

The author acknowledges the assistance of Richard Hay, who introduced her to the zeolites of Olduvai and who assisted and advised her on the earliest stages of this project. She is also grateful to the Tanzania Commission for Science and Technology (COSTECH) and the Tanzania Antiquities Department for granting her permission to conduct field research at Olduvai Gorge. Harald Stollhofen, Ian Stanistreet, Gail Ashley, Carl Swisher, Godwin Mollel, Robert Blumenschine, other past and present members of the Olduvai Landscape Archaeology and Paleoanthropology Project (directed by R. Blumenschine, F. Masao, and J. Njau), Jeremy Delaney, John Fournelle, Kiel Finn, Victoria Hover, and Heather Owen provided invaluable support for both the field and analytical portions of this project. Funding was provided by the L.S.B. Leakey Foundation, the Geological Society of America, Sigma Xi, the National Science Foundation (Ashley: EAR-9903258, field expenses; Swisher: BCS-0109027, field expenses; Owen: MRI-0723002, purchased the Hitachi SEM and Bruker EDS used in this project), the University of Wisconsin-Milwaukee Research Growth Initiative, and the American Chemical Society Petroleum Research Fund.

REFERENCES

Boles, J.R. and Coombs, D.S. (1975) Mineral reactions in zeolitic Triassic tuff, Hokonui Hills, New Zealand. *Bulletin of the Geological Society of America*, **86**, 163–173.

Broxton, D.E., Bish, D.L., and Warren, R.G. (1987) Distribution and chemistry of diagenetic minerals at Yucca Mountain, Nye County, Nevada. *Clays and Clay Minerals*, **35**, 89–110.

Chipera, S.J. and Apps, J.A. (2001) Geochemical stability of natural zeolites. Pp. 117–161 in: *Natural Zeolites: Occurrence, Properties, Applications* (D.L. Bish and D.W. Ming, editors). Reviews in Mineralogy and Geochemistry, **45**, Mineralogical Society of America, Washington, D.C.

Chipera, S.J., Goff, F., Goff, C.J., and Fittipaldo, M. (2008) Zeolitization of intercaldera sediments and rhyolitic rocks in the 1.25 Ma lake of Valles caldera, New Mexico, USA. *Journal of Volcanology and Geothermal Research*, **178**, 317–330.

Deocampo, D.M. (2004) Authigenic clays in East Africa: Regional trends and paleolimnology at the Plio-Pleistocene boundary, Olduvai Gorge, Tanzania. *Journal of Paleolimnology*, **31**, 1–9.

Deocampo, D.M., Blumenschine, R.J., and Ashley, G.M. (2002) Wetland diagenesis and traces of early hominids, Olduvai Gorge, Tanzania. *Quaternary Research*, **57**, 1–11.

Dibble, W.E. Jr. and Tiller, W.A. (1981) Kinetic model of zeolite paragenesis in tuffaceous sediments. *Clays and Clay Minerals*, **29**, 323–330.

Donovan, J. (2000) *Probe for Windows: Analysis and Automation for EPMA, version 5.11*. Software package distributed by Advanced Microbeam, Vienna, Ohio, USA.

Drief, A. and Schiffman, P. (2004) Very low temperature alteration of sideromelane in hyaloclastites and hyalotuffs from Kilauea and Mauna Kea volcanoes: implications for the mechanism of palagonite formation. *Clays and Clay Minerals*, **52**, 622–634.

Franzson, H., Zierenberg, R., and Schiffman, P. (2008) Chemical transport in geothermal systems in Iceland. Evidence from hydrothermal alteration. *Journal of Volcanology and Geothermal Research*, **173**, 217–229.

Grant, J.A. (1986) The isocon diagram – a simple solution to Gresens' equation for metasomatic alteration. *Economic Geology*, **81**, 1976–1982.

Grant, J.A. (2005) Isocon analysis: A brief review of the method and applications. *Physics and Chemistry of the Earth*, **30**, 997–1004.

Hay, R.L. (1963) Zeolitic weathering in Olduvai Gorge, Tanganyika. *Geological Society of America Bulletin*, **74**, 1281–1286.

Hay, R.L. (1964) Phillipsite of saline lakes and soils. *American Mineralogist*, **49**, 1366–1387.

Hay, R.L. (1966) *Zeolites and Zeolitic Reactions in Sedimentary Rocks*. Geolocial Society of America, Special Paper **85**, Geological Society of America, New York.

Hay, R.L. (1970) *Silicate reactions in three lithofacies of a semi-arid basin, Olduvai Gorge, Tanzania*. Mineralogical Society of America, Papers, **3**, 237–255.

Hay, R.L. (1973) Lithofacies and environments of Bed I, Olduvai Gorge, Tanzania. *Quaternary Research*, **3**, 541–560.

Hay, R.L. (1976) *Geology of the Olduvai Gorge: A Study of Sedimentation in a Semiarid Basin*. University of California Press, Berkeley, California, USA.

Hay, R.L. (1980) Zeolitic weathering of tuffs in Olduvai Gorge, Tanzania. Pp. 155–163 in: *Proceedings of the Fifth International Conference on Zeolites: Naples, Italy, 1–6 June 1980* (L.V.C. Rees, editor). Heyden, London.

Hay, R.L. (1986) Geologic occurrence of zeolites and some associated minerals. *Pure and Applied Chemistry*, **58**, 1339–1342.

Hay, R.L. (1996) Stratigraphy and Lake-margin Paleoenvironments of Lowermost Bed II in Olduvai Gorge. *Kaupia-Darmstädter Beiträge zur Naturgeschichte* **6**, 223–230.

Hay, R.L. and Guldman, S.G. (1987) Diagenetic alteration of silicic ash in Searles Lake, California. *Clays and Clay Minerals*, **35**, 449–457.

Hay, R.L. and Kyser, T.K. (2001) Chemical sedimentology and paleoenvironmental history of Lake Olduvai, a Pliocene lake in northern Tanzania. *Geological Society of America Bulletin*, **113**, 1505–1521.

Hay, R.L. and Sheppard, R.A. (2001) Occurrences of zeolites in sedimentary rocks: an overview. Pp. 216–234 in: *Natural Zeolites: Occurrence, Properties, Applications* (D.L. Bish and D.W. Ming, editors). Reviews in Mineralogy and Geochemistry, **45**, Mineralogical Society of America, Washington, D.C.

Hover, V.C. and Ashley, G.M. (2003) Geochemical signatures of paleodepositional and diagenetic environments: A STEM/AEM study of authigenic clay minerals from an arid rift basin, Olduvai Gorge, Tanzania. *Clays and Clay Minerals*, **51**, 231–251.

Jones, B.F. and Deocampo, D.M. (2003) Geochemistry of Saline Lakes. Pp. 393–424 in: *Surface and Ground Water, Weathering, Erosion, and Soils* (J.I. Drever, editor). *Treatise on Geochemistry*, Vol. **5**, Elsevier, New York.

Jones, B.F. and Weir, A.H. (1983) Clay minerals of Lake Albert, an alkaline, saline lake. *Clays and Clay Minerals*, **34**, 161–172.

Langella, A., Cappelletti, P., and de'Gennaro, M. (2001) Zeolites in closed hydrologic systems. Pp. 235–260 in: *Natural Zeolites: Occurrence, Properties, Applications* (D.L. Bish and D.W. Ming, editors). Reviews in Mineralogy and Geochemistry, **45**, Mineralogical Society of America, Washington, D.C.

McHenry, L.J. (2004) Characterization and correlation of altered Plio-Pleistocene tephra using a "multiple technique" approach: Case study at Olduvai Gorge, Tanzania. PhD dissertation, Rutgers University, New Brunswick, New Jersey, USA, 392 pp.

McHenry, L.J. (2005) Phenocryst composition as a tool for correlating fresh and altered tephra, Bed I, Olduvai Gorge, Tanzania. *Stratigraphy*, **2**, 101–115.

McHenry, L.J. (2009) Element mobility during zeolitic and argillic alteration of volcanic ash in a closed-basin lacustrine environment: Case study Olduvai Gorge, Tanzania. *Chemical Geology*, **265**, 540–552.

McHenry, L.J. (in press) A revised stratigraphic framework for Olduvai Gorge Bed I based on tuff geochemistry. *Journal of Human Evolution*.

McHenry, L.J., Mollel, G.M., and Swisher, C.C. III (2008) Compositional and textural correlations between Olduvai Gorge Bed I tephra and volcanic sources in the Ngorongoro Volcanic Highlands, Tanzania. *Quaternary International*, **178**, 306–319.

Mees, F., Stoops, G., Van Ranst, E., Paepe, R., and Van Overloop, E. (2005) The nature of zeolite occurrences in deposits of the Olduvai Basin, Northern Tanzania. *Clays and Clay Minerals*, **53**, 659–673.

Mees, F., Segers, S., and Van Ranst, E. (2007) Palaeoenvironmental significance of the clay mineral composition of Olduvai basin deposits, northern Tanzania. *Journal of African Earth Sciences*, **47**, 39–48.

Ming, D.W. and Mumpton, F.A. (1989) Zeolites in soils. Pp. 837–911 in: *Minerals in Soil Environments* (J.B. Dixon and S.B. Weed, editors). SSSA Books, **1**, Soil Society of America, Madison, Wisconsin, USA.

Moore, D.M. and Reynolds, R.C. Jr. (1997) *X-ray Diffraction and the Identification and Analysis of Clay Minerals*. 2nd edition. Oxford University Press, Oxford, UK.

Passaglia, E. (1970) The crystal chemistry of chabazites. *American Mineralogist*, **55**, 1278–1301.

Pe-Piper, G. and Tsolis-Katagas, P. (1991) K-rich mordenite from Late Miocene rhyolitic tuffs, island of Samos, Greece. *Clays and Clay Minerals*, **39**, 239–247.

Renaut, R.W. (1993) Zeolitic diagenesis of late Quaternary fluviolacustrine sediments and associated calcrete formation in the Lake Bogoria Basin, Kenya Rift Valley. *Sedimentology*, **40**, 271–301.

Sheppard, R.A., Gude, A.J., and Fitzpatrick, J.J. (1988) Distribution, characterization, and genesis of mordenite in Miocene silicic tuffs at Yucca Mountain, Nye County, Nevada. *U.S. Geological Survey Bulletin*, **1777**, 22 pp.

Sheppard, R.A. and Hay, R.L. (2001) Formation of zeolites in open hydrologic systems. Pp. 261–275 in: *Natural Zeolites: Occurrence, Properties, Applications* (D.L. Bish and D.W. Ming, editors). Reviews in Mineralogy and Geochemistry, **45**, Mineralogical Society of America, Washington, D.C.

Snellings, R., Van Haren, T., Machiels, L., Mertens, G., Vandenberghe, N., and Elsen, J. (2008) Mineralogy, geochemistry, and diagenesis of clinoptilolite tuffs (Miocene) in the central Simav graben, western Turkey. *Clays and Clay Minerals*, **56**, 622–632.

Stollhofen, H., Stanistreet, I.G., McHenry, L.J., Mollel, G.F., Blumenschine, R.J., and Masao, F.T. (2008) Fingerprinting facies of the Tuff IF marker, catastrophe for early hominin palaeoecology, Olduvai Gorge, Tanzania. *Palaeogeography, Palaeoclimatology, Palaeoecology*, **259**, 382–409.

Surdam, R.C. and Eugster, H.P. (1976) Mineral reactions in the sedimentary deposits of the Lake Magadi region, Kenya. *Geological Society of America Bulletin*, **87**, 1739–1752.

Taylor, M.W. and Surdam, R.C. (1981) Zeolite reactions in the tuffaceous sediments at Teels Marsh, Nevada. *Clays and Clay Minerals*, **29**, 341–352.

(*Received 5 February 2010; revised 9 September 2010; Ms. 408; A.E. R.J. Pruett*)